Numerical Methods in Civil Engineering, 10-1 (2025) 13-22

Numerical Methods in Civil Engineering

Journal Homepage: https://nmce.kntu.ac.ir/

Modeling the effect of unsaturated conditions on chloride penetration in one-part alkali-activated slag concrete

Ali Sadrmomtazi*, Hamed Zanganeh**

ARTICLE INFO

RESEARCH PAPER

Article history:
Received:
July 2025
Revised:
August 2025
Accepted:
August 2025

Keywords:
one-part alkali-activated slag concrete, unsaturated conditions, rapid chloride migration test, finite difference approach, corrosion initiation time;

Abstract:

In this study, the effect of unsaturated conditions and curing time before exposure to an unsaturated environment on the properties of one-part alkali-activated slag concrete (O-AAS) and Ordinary Portland cement concrete (OPCC) was investigated. The samples were cured in water saturated with alkaline materials for 7, 28, 56, and 360 days. However, the specimens cured for 7, 28, and 56 days were stored in an unsaturated environment with 50% relative humidity until they reached 360 days of age. Compressive strength and rapid chloride migration tests (RCMT) were conducted at various ages up to 360 days, and corrosion initiation time was estimated by solving Fick's second law using the finite difference approach and results from RCMT.

Results show that reducing the curing time before unsaturated exposure significantly decreased O-AAS's compressive strength and increased its chloride ion diffusion coefficient more significantly than OPCC. Chloride penetration modeling indicates that exposure to an unsaturated environment has a more pronounced effect on reducing the corrosion initiation time of O-AAS compared to OPCC. Also, increasing the curing time from 7 days to 56 days before exposure to an unsaturated environment caused a 186.7% increase in the estimated corrosion initiation time of O-AAS and a 20.4% increase in the estimated corrosion initiation time of OPCC. The required curing time for the O-AAS mixture to eliminate the effect of an unsaturated environment with a relative humidity of 50% on the compressive strength and chloride ion diffusion coefficient on standard specimens is 56 days, and for the OPCC mixture is 28 days.

Nomenclature list

O-AAS: One-part alkali-activated slag concrete
OPCC: Ordinary Portland cement concrete
GGFBS: Ground granulated blast furnace slag
RCMT: Rapid Chloride Migration Test
RH: Relative Humidity
SSD: Saturated Surface Dry
D_{nssm}: Non-steady-state diffusion coefficient coefficient($\times 10^{-12}$ $m^2/_s$)
T : Average of the initial and final temperatures in the sodium chloride solution (°C)
U : Absolute value of the applied voltage (V);
L : Thickness of the specimen (mm)
x_d: Average value of the penetration depths (mm)
t_d : Test duration (hours)
C(x,t): The chloride concentration (%wt of concrete)
x : The depth below the exposed surface (m)
t: The exposure time (s)
$D(t)$: The diffusion coefficient of chlorides ($m^2/_s$)
$r = D(t)\frac{dt}{2(dx)^2}$: The dimensionless Courant–Friedrichs–Lewy (CFL) number
dx : The distance increment
dt : The time step
u_i^t is : chloride concentration at time t and slice I (%wt of concrete)
D_{ref} : the concrete diffusion coefficient at time t_{ref}
m : the aging factor
RMSE: Root Mean Squared Error

* *Professor, Department of Civil Engineering, Faculty of Engineering, University of Guilan, Rasht, Iran*
** *Corresponding author: Ph.D. Candidate, Department of Civil Engineering, Faculty of Engineering, University of Guilan, Rasht, Iran. E-mail:hamedzanganeh@gmail.com*

https://doi.org/10.61882/NMCE.2506.1094

1. Introduction

Chloride ion penetration and reinforcement corrosion are major concerns for reinforced concrete structures exposed to chloride environments. Therefore, investigating and modeling the phenomenon of chloride ion penetration in concrete, especially modern concretes such as alkali-activated concretes, is of interest to researchers [1,2]. Several analytical and numerical methods have been developed for modeling chloride ion diffusion in concrete. The finite difference numerical method is one of the widely used approaches for modeling chloride ion penetration in concrete by solving Fick's second law [3-5]. In the present study, chloride ion penetration in alkali-activated slag concrete is modeled using a one-dimensional Crank-Nicolson finite difference approach and compared with Ordinary Portland cement concrete.

Understanding and accurately predicting the long-term performance, particularly concerning durability against chloride ingress, is crucial for the wider adoption of alkali-activated concretes.

Using alkali-activated concrete can provide many environmental benefits. This has drawn the attention of researchers in recent years to accurately understand the behavior of alkali-activated concrete in various environmental conditions in order to develop their application fields in industry [6,7]. The environmental conditions of concrete in structures such as bridge decks or precast elements are such that, after curing, it remains in unsaturated conditions for a period of time and is then exposed to chloride environments.

Exposure of concrete to unsaturated environments leads to moisture loss from pores and, over time, causes deformation in the paste, resulting in volumetric instability [8-11]. The volumetric stability of aggregates prevents paste shrinkage, leading to stress development at the aggregate–paste interface. As paste shrinkage increases, these stresses intensify, eventually exceeding the paste's tensile strength and causing microcracks in the internal body and surface of the concrete [12-14]. Both alkali-activated slag concrete and Ordinary Portland cement concretes are susceptible to drying shrinkage-induced microcracking. Nevertheless, alkali-activated slag concrete experiences notably greater drying shrinkage due to its finer pore structure and higher density, leading to a more pronounced risk of microcrack formation compared to Ordinary Portland cement concretes [10,11].

Previous research results indicate that microcracks caused by storing concrete specimens in an unsaturated environment after proper curing did not have a significant effect on the compressive strength of Ordinary Portland cement concrete[15-17]. In contrast to compressive strength, unsaturated conditions can significantly increase the permeability of Ordinary Portland cement concrete[12,17,18]. For alkali-activated slag concretes, some studies have reported considerable reductions in compressive strength after unsaturated exposure. However, previous studies show considerable variation in the reported compressive strength loss of alkali-activated slag concrete exposed to unsaturated conditions. A thorough analysis of previous studies indicates that both the ambient relative humidity and the curing duration before exposure to unsaturated conditions significantly affect the compressive strength reduction in alkali-activated slag concrete[14,19-23].

Despite growing interest in O-AAS concrete for sustainable construction, a knowledge gap still exists regarding its long-term durability in unsaturated conditions. Most existing studies evaluate chloride ingress immediately after curing, which do not reflect real-world conditions where concrete may be exposed to drying before coming into contact with chloride environments. Crucially, the combined effect of variable initial curing durations followed by unsaturated exposure on the subsequent chloride resistance and corrosion initiation time of O-AAS has not been systematically investigated. This study addresses this gap by experimentally evaluating the influence of curing duration (7, 28, and 56 days) followed by 50% RH exposure on the compressive strength and chloride diffusion coefficient of O-AAS, in direct comparison with OPC concrete; and by applying a Crank-Nicolson-based finite difference model using the experimental results to investigate the long-term durability of OPCC and OAAS concretes with respect to microcracks induced by drying shrinkage.

2. Experimental Program

2.1 Materials

The binder materials used were Type II Portland cement (Nahavand Cement Company, conforming to ASTM C150 [24]); Grade 100 ground granulated blast furnace slag (GGBFS) from Esfahan Steel Company (in accordance with ASTM C989 [25]); and anhydrous sodium metasilicate powder from Qingdao Darun Chemical Company, in China. The chemical compositions and physical properties of these binders are presented in Tables 1 and 2, respectively.

The aggregates used in this study were sourced from quarries located in the southwest of Tehran. Coarse aggregate (gravel) had a nominal maximum size of 12.5 mm, and the fine aggregate (sand) met the requirements of ASTM C33 [26]. The percentage passing the No. 200 sieve was 1.88% for sand and 0.21% for gravel. The water absorption (saturated surface dry basis) and saturated surface dry density were 1.8% and 2590 kg/m³ for gravel, and 3.7% and 2510 kg/m³ for sand, respectively. Tap water from Tehran’s

municipal supply was used for all concrete mixing operations.

Table 1: Chemical Analysis Results of Binding Materials.

%	Cement	GGBFS	Anhydrous sodium metasilicate
SiO_2	20.80	35.92	46.2
Al_2O_3	4.80	11.91	-
Fe_2O_3	4.00	0.62	-
CaO	63.70	38.38	-
MgO	2.10	8.89	-
SO_3	2.40	0.59	-
Na_2O	0.37	0.57	50.8
K_2O	0.85	0.96	-
L.O.I.	0.96	1.08	-

Table 2: Physical properties of Binding Materials.

Binding Materials	Physical Properties		Value	Unit
Cement	Specific Gravity		3.14	gr/cm^3
	Fineness, Blaine		3350	cm^2/gr
	Initial Setting		195	min
	Final Setting		270	min
	Compressive strength	7 day	360	kg/cm^2
		28 day	428	kg/cm^2
GGBFS	Specific Gravity		2.82	gr/cm^3
	Fineness, Blaine		4010	cm^2/gr
	Residue on 45 µm Sieve		8.0	**%**
	Activity Index	7 day	88	**%**
		28 day	108	**%**
Anhydrous sodium metasilicate	Specific Gravity		1.20	gr/cm^3
	Water-Insoluble materials		0.12	**%**

2.2 Mix Design and Testing Procedures

Concrete mixtures were produced with a binder content of 450 kg/m^3 and a water-to-binder ratio of 0.52. The properties of the studied mixtures are presented in Table 3. In this report, Ordinary Portland cement mixtures are labeled as OPCC, while One-part alkali-activated slag concrete mixtures are labeled as O-AAS.

Table 3: Mix Design Components.

Mix ID	OPCC	O-AAS
Cement (kg/m^3)	450.0	-
Slag (kg/m^3)	-	405.0
Anhydrous sodium metasilicate (kg/m^3)	-	45.0
Fine Aggregate SSD (kg/m^3)	1001.0	975.0
Coarse Aggregate SSD (kg/m^3)	539.0	525.0
W/B	0.52	0.52
Concrete temperature (ºC)	23.1	26.1

For the mixing process, solid components (including aggregates and binder powder) were first dry-mixed in the mixer for 2 minutes. Water was then added, followed by 3 minutes of mixing. The mixer was stopped for 3 minutes, after which mixing resumed for another 3 minutes before a 2-minute pause. Finally, the mixture was mixed for a further 3 minutes.

Cylindrical specimens (10×20 cm) were cast and stored for 24 hours in an environment with ≥95% relative humidity. Saturated limewater solution was used for OPCC specimens, while sodium metasilicate-saturated solution was used for O-AAS specimens. The use of a sodium metasilicate-saturated solution for O-AAS specimens was chosen to prevent the leaching of alkali ions and maintain a high pH in the surrounding environment. This condition minimizes the concentration gradient between the pore solution and the external medium, thereby preserving the activator. This approach is consistent with the findings of Marvila et al. [27], who demonstrated that curing in an alkaline-rich solution (e.g., sodium hydroxide) prevents ion loss and yields superior mechanical performance compared to curing in distilled water. Similarly, saturated limewater is the standard curing method for OPCC to prevent decalcification.

The four storage conditions for the specimens from the time of removal from demolding until testing are:

-W: Continuous immersion in 23°C solution

-W7A: 6-day immersion in 23°C solution, then transferred to 50% RH at 23°C

-W28A: 27-day immersion in 23°C solution, then transferred to 50% RH at 23°C

-W56A: 55-day immersion in 23°C solution, then transferred to 50% RH at 23°C

The selected unsaturated conditions are similar to the moisture conditions specified in the ASTM C157 [28] standard test for determining the length change of specimens due to drying shrinkage.

The compressive strength test was conducted according to the ASTM C39 [29] standard on three cylindrical specimens (10×20 cm) at ages of 28, 56, 90, 180, and 360 days. Before the compressive strength test, the specimen ends were capped using sulfur mortar.

The RCMT was performed according to the NT Build 492 [30] on three specimens at ages of 28, 56, 90, 180, and 360 days. For specimens taken directly from the alkaline saturation solution at the time of testing, preparation steps (cutting and saturation) were performed according to the standard.

However, for specimens exposed to an unsaturated environment before their testing age, the following procedure was adopted: After curing in the alkaline-saturated solution, a 2.5 cm-thick disk was cut from each 10x20 cm cylindrical specimen, discarding the troweled surface. These cut disks were set aside. The remaining cylinder was then stored in an unsaturated environment with 50% relative humidity and 23°C until the time of testing. At the time of testing, a 5 cm-thick disk was sectioned from the previously cut surface of each remaining cylinder and subsequently saturated according to the standard method.

During the test, one side of each specimen was exposed to a 10% sodium chloride solution, while the opposite side was subjected to a 0.3 N sodium hydroxide solution. To accelerate chloride ion penetration, an electrical potential was applied, with the voltage determined based on the initial current passing through the specimen.

After the test, the specimens were split, and a 0.1 N silver nitrate solution was applied to the exposed surfaces. The silver nitrate reacted with the chlorides, forming white silver chloride, which marked the chloride penetration front. This visible boundary was used to identify the extent of chloride penetration, and the migration coefficient was then calculated using Equation 1 [29].

$$D_{nssm} = \frac{0.0239(273+T)L}{(U-2)t_d}\left(x_d - 0.0238\sqrt{\frac{(273+T)Lx_d}{U-2}}\right) \quad (1)$$

Where:

D_{nssm}= Non-steady-state diffusion coefficient$\left(\times 10^{-12}\, m^2/_S\right)$;

U = Absolute value of the applied voltage (V);

T = Average of the initial and final temperatures in the sodium chloride solution ($^{\circ}C$);

L = Thickness of the specimen (mm);

x_d= Average value of the penetration depths (mm);

t_d = Test duration $(hours)$.

Additionally, to obtain the parameters required for modeling the W7A, W28A, and W56A exposure conditions, some specimens from each curing regime were transferred from the unsaturated environment to the saturated condition at 90 days. The RCMT was then performed on these specimens at 180 and 360 days. This approach was chosen because the modeling assumes fully saturated concrete conditions after exposure to the chloride environment.

3. Results and Discussion

3.1 Compressive Strength

The compressive strength results of the mixtures under different curing conditions are presented in Figure 1. For this study, O-AAS mix proportions were specifically designed to achieve 28-day compressive strength comparable to Ordinary Portland cement concrete mixtures under alkaline solution curing, based on findings by Rahmani et al. [31].

Generally, when comparing O-AAS and OPCC under identical curing and environmental conditions, their compressive strength development trends over time differ significantly.

The compressive strength of OPCC under W conditions at 28, 56, 90, 180, and 360 days was 37.7, 41.1, 45.3, 47.9, and 48.6 MPa, respectively. As shown in Figure 1, the compressive strength of OPC increased over time under all tested conditions, with similar trends observed for W, W7A, W28A, and W56A.

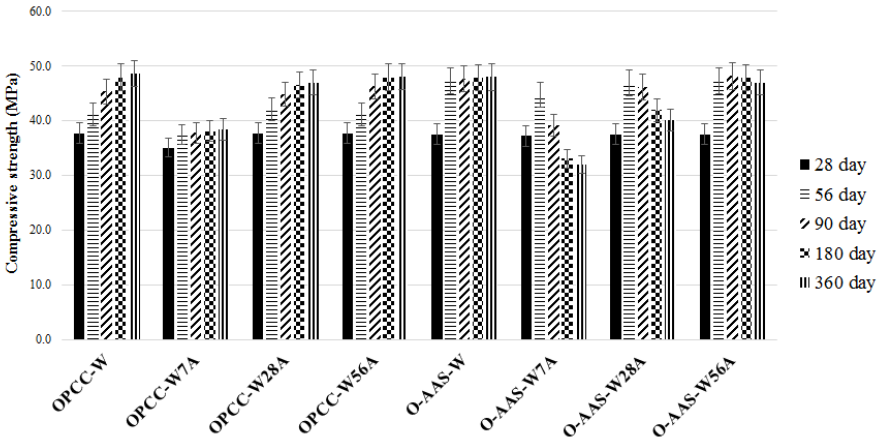

Fig. 1: The development of compressive strength under varying environmental conditions over time.

The 360-day compressive strengths of OPCC specimens under W, W7A, W28A, and W56A conditions were 48.6, 38.4, 47.0, and 48.1 MPa, respectively. Notably, the long-term (360-day) compressive strengths in W, W28A, and W56A were nearly identical, while W7A exhibited a 21.0% lower strength compared to W conditions.

The compressive strength of O-AAS under W conditions at 28, 56, 90, 180, and 360 days was 37.5, 47.3, 47.5, 47.8, and 47.9 MPa, respectively. Under W7A conditions, the corresponding strengths were 37.1, 44.9, 39.9, 34.4, and 33.6 MPa. The results indicate that unsaturated conditions significantly affect the compressive strength of O-AAS (alkali-activated slag). The 360-day compressive strength under W7A conditions shows:

-A 28.3% reduction compared to its peak strength at 56 days

-A 33.2% reduction relative to the 360-day strength under W conditions.

The 360-day compressive strength of AAS under W28A and W56A conditions is 16.3% and 2.0% lower than that under W conditions, respectively. Figure 1 also shows that the variations in compressive strength of AAS under W and W56A conditions are similar, increasing up to 56 days of age

and then stabilizing. However, the compressive strength under W7A and W28A conditions increases up to 56 days of age and then decreases at later ages. The primary reason for the reduction in compressive strength of alkali-activated slag mixtures in unsaturated environments is the formation of microcracks due to drying shrinkage [14,21].

Therefore, the required curing duration to prevent the formation of microcracks caused by drying shrinkage at a relative humidity of 50% has a greater impact on the compressive strength of O-AAS mixtures compared to OPCC mixtures. The obtained results indicate that to eliminate the effect of the unsaturated environment with a relative humidity of 50% on the one-year compressive strength of OPCC and O-AAS mixtures, the required durations are 28 and 56 days, respectively.

In the report by Collins and Sanjayan [14], the compressive strength of alkali-activated slag concrete that was placed in an unsaturated environment after demolding was investigated. According to this report, the one-year compressive strength of the concrete in an unsaturated environment with 50% relative humidity decreased by approximately 54% compared to saturated conditions. Furthermore, in the unsaturated environment, its one-year compressive strength experienced a 17% reduction compared to the maximum strength achieved at earlier ages. In the study by Prinsse et al. [21], the compressive strength of alkali-activated slag concrete in an unsaturated environment with 55% relative humidity was examined after 28 days of curing in water. The compressive strength increased by approximately 5% up to 91 days and decreased by about 7% at 695 days. The results of the aforementioned studies also confirm the findings of the present research.

3.2 Chloride diffusion coefficient

Figure 2 presents the chloride ion diffusion coefficients obtained from the Rapid Chloride Migration Test (RCMT). In all examined mixtures, the chloride ion diffusion coefficient decreased with increasing age. Our results indicate that exposing both OPCC and O-AAS mixtures to an unsaturated environment significantly increases the chloride ion diffusion coefficient, though the extent of this effect varies for each mixture.

Under W conditions, the OPCC mixture's chloride ion diffusion coefficient at 28, 56, 90, 180, and 360 days was 22.4, 19.1, 17.7, 14.4, and 12.8 $\times 10^{-12}$ m²/s, respectively.

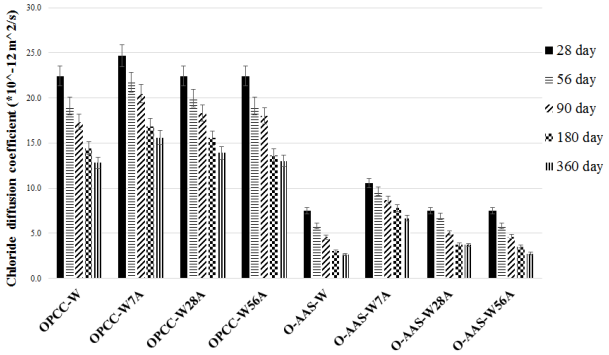

Fig. 2: Chloride diffusion coefficient of mixtures under varying conditions and over time.

The W7A conditions resulted in a significant increase in OPCC's diffusion coefficient compared to W conditions. Specifically, at 360 days, the W7A OPCC mixture showed an increase of approximately 22% compared to W conditions. Extending the curing period before unsaturated exposure from 7 to 28 days substantially reduced the enhancing effect of the 50% RH environment on the chloride ion diffusion coefficient. Furthermore, OPCC's chloride ion diffusion coefficient under W56A conditions was very similar to that under W conditions.

Under W conditions, the AAS mixture's chloride ion diffusion coefficient at 28, 56, 90, 180, and 360 days was 7.5, 5.8, 4.6, 3.0, and 2.6 $\times 10^{-12}$ m²/s, respectively. This demonstrates that the 360-day AAS mixture under W conditions exhibits a chloride ion diffusion coefficient significantly lower than that of the OPCC mixture (approximately 80% lower than OPCC at 360 days).

For O-AAS, the 360-day chloride ion diffusion coefficients under W7A, W28A, and W56A conditions were 2.55, 1.41, and 1.05 times higher than under W conditions, respectively. These findings confirm that extending the curing period before exposure to a 50% relative humidity environment can significantly reduce the negative effect of the unsaturated environment. This is attributed to increased resistance to shrinkage-induced stresses with longer curing, resulting in fewer micro-cracks.

Moreover, these results indicate that exposure to unsaturated conditions has a greater impact on the chloride ion diffusion coefficient of O-AAS mixtures compared to OPCC mixtures. This heightened effect in O-AAS is likely due to its inherently higher drying shrinkage compared to OPCC, leading to a more pronounced formation of micro-cracks in O-AAS mixtures under unsaturated conditions [10].

3.3 Numerical Model

The modeling of chloride ion penetration into concrete has been extensively performed using Fick’s second law (Equation 2) [3-5]. Various analytical and numerical methods have been proposed to solve this equation.

$$\frac{dC(x,t)}{dt} = D(t)\frac{d^2C(x,t)}{dx} \quad (2)$$

Here, $C(x,t)$ represents the chloride concentration (as a percentage of the concrete's mass) at a depth x and the time t, x is the depth below the exposed surface (m),t is the exposure time (s), and $D(t)$ is the diffusion coefficient of chlorides $(\frac{m^2}{s})$.

In one-dimensional conditions, considering an element based on the Crank-Nicolson finite difference method, the equation can be rewritten as Equation 3 [5].

$$-ru_{i+1}^{t+1} + (1+2r)u_i^{t+1} - ru_{i-1}^{t+1} = ru_{i+1}^{t} + (1-2r)ru_i^{t} + ru_{i-1}^{t} \quad (3)$$

Here, $r = D(t)\frac{dt}{2(dx)^2}$ represents the dimensionless Courant–Friedrichs–Lewy (CFL) number, $D(t)$ is the diffusion coefficient at time t $(\frac{m^2}{s})$, dx is the distance increment (total depth divided by number of slices), dt is the time step (s), and u_i^t is the chloride concentration (%wt of concrete) at time *t* and slice *i*, i =1, …, I is the particular slice of concrete (and *i* = 0 is the top slice that holds the external concentration of chlorides), t is the time (s).

Figure 3 presents a detailed flowchart of the Crank-Nicolson finite difference method implementation, illustrating the step-by-step numerical procedure for solving Fick's second law and predicting chloride ion penetration in concrete.

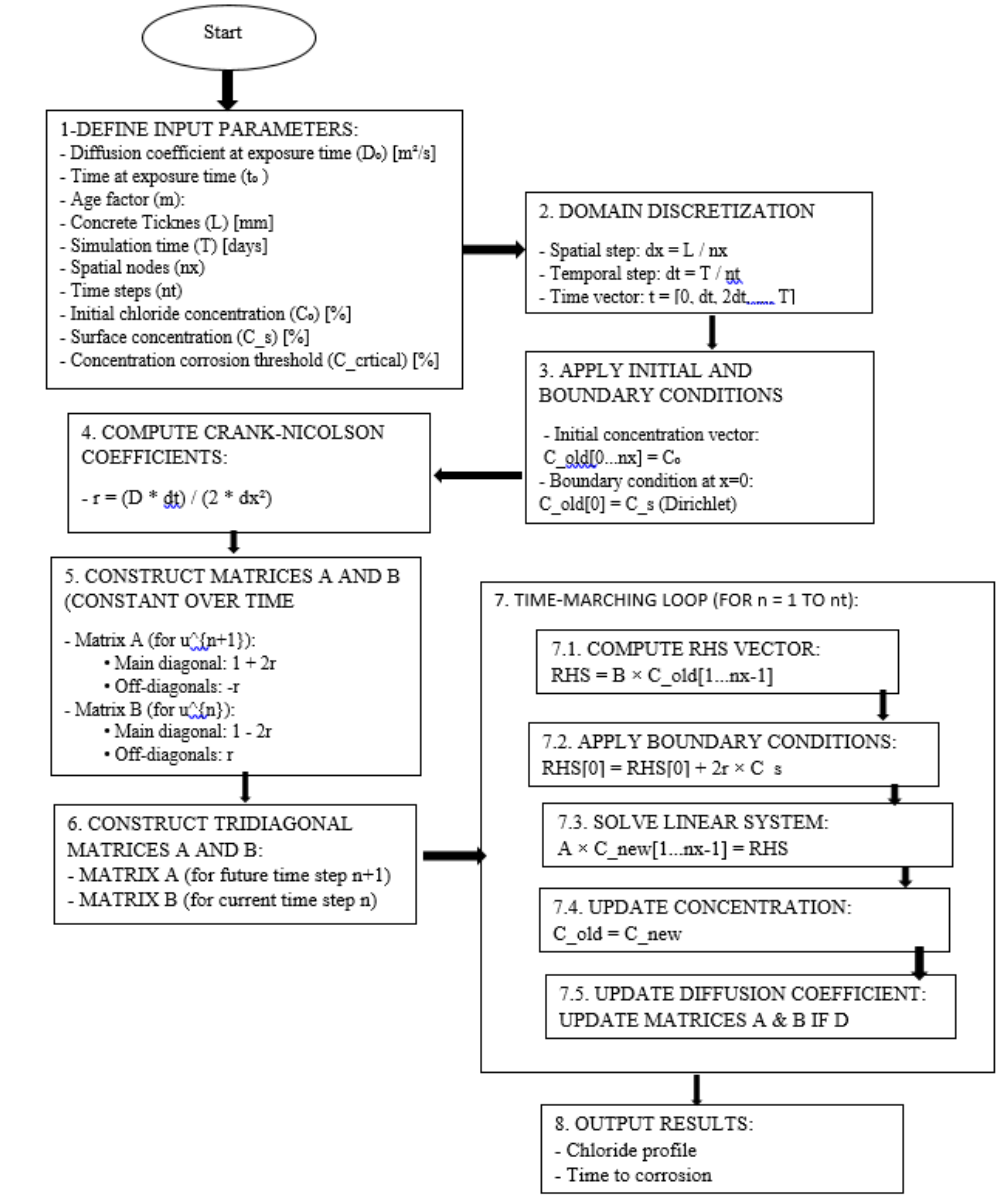

Fig. 3: Step-by-Step Implementation of Crank-Nicolson Scheme for Fick's Second Law

The Crank–Nicolson method was employed to evaluate the resistance of concrete to chloride ion penetration, using data derived from the Rapid Chloride Migration (RCM) tests [3,4]. The temporal variation in the chloride diffusion coefficient was determined according to Equation 4 [3,4]:

$$D(t) = D_{ref}\left(\frac{t_{ref}}{t}\right)^{m} \quad (4)$$

In this equation, $D(t)$ represents the concrete's diffusion coefficient at time t, D_{ref} is the concrete diffusion coefficient at time t_{ref}, and m is the aging factor.

In this study, environmental conditions such as temperature were considered identical and constant during the period of exposure of the mixtures to the chloride environment. Additionally, a constant chloride diffusion coefficient was assumed across the concrete cross-section. The research investigates the effects of age, curing conditions, and prior exposure to an unsaturated environment before contact with the chloride environment.

The surface chloride concentration was set at a constant 0.8% of the concrete's weight in this study [3,4]. For comparison, in the Life 365 software, the surface chloride concentration is also fixed at 0.8% for specific submerged conditions [5].

In this study, the age of concrete at the time of exposure to the chloride environment was considered to be 90 days. For modeling and determining the age factor under W7A, W28A, and W56A conditions, RCMT results from specimens transferred to a saturated environment after 90 days of age were used. The results of the obtained diffusion coefficients for these specimens are presented in Figure 4. Using the results from the RCMT, the age factor and chloride ion diffusion coefficient used in the modeling were determined for each mixture, and the results are provided in Table 4. Notably, the age factor obtained in this study is consistent with the results from Bagheri et al. [3,32] and the Life-365 software's model [5].

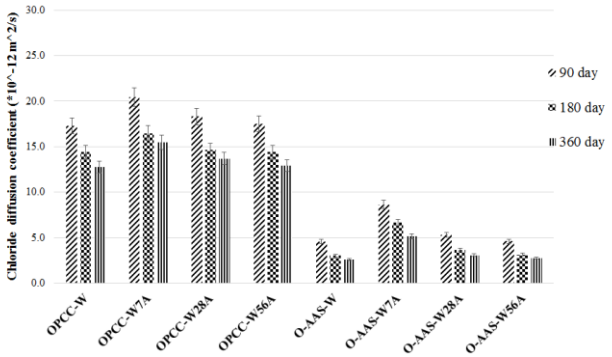

Fig. 4: The chloride diffusion coefficient of mixtures used in modeling

Table 4: The aging factors and diffusion coefficients employed in the modeling process.

Mix Destination	m	D_{ref} ($\times 10^{-12}\ \frac{m^2}{s}$)
OPCC-W	0.218	17.31
OPCC-W7A	0.202	20.47
OPCC-W28A	0.210	18.32
OPC-W56A	0.218	17.48
AAS-W	0.403	4.56
AAS-W7A	0.372	8.65
AAS-W28A	0.398	5.31
AAS-W56A	0.402	4.62

3.4 Model Validation

To evaluate the reliability and accuracy of the developed numerical model in predicting chloride penetration into concrete, a validation process was conducted by comparing the model outputs with experimental chloride concentration profiles obtained from data analysis.

Chloride concentration profiles for OPCC with a water-to-binder ratio of 0.50, exposed to chloride ingress for durations ranging from 28 to 180 days under laboratory conditions in accordance with ASTM C1556, were extracted from the study by Bagheri et al. [32]. As illustrated in Figure 5, the chloride concentration profile predicted by the numerical model for the OPCC-W condition was compared with the experimental data at 180 days. The numerical model demonstrates good agreement with experimental data, achieving an RMSE of 0.1205% and an R^2 of 0.912, indicating that approximately 91.2% of the variability in chloride concentration is captured by the model. The results confirm the model's capability in simulating chloride ingress in OPCC under submerged conditions.

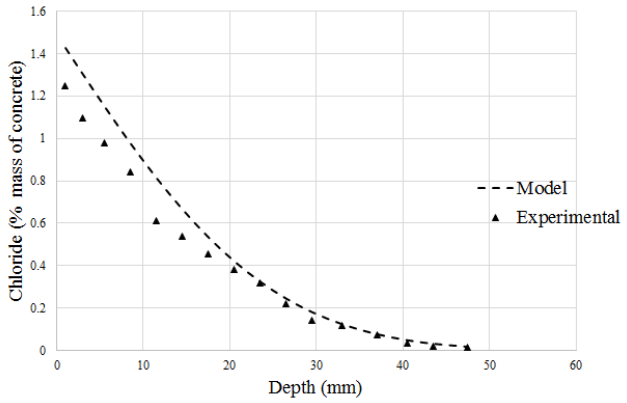

Fig. 5: Chloride concentration profile (in % by weight of concrete) predicted by the model vs. experimental data at 180 days.

A portion of the observed discrepancy can be attributed to the slight difference in the water-to-binder ratio between the two studies (0.50 in Bagheri et al. versus 0.52 in the present study), which influences the chloride diffusion coefficient. It should be noted that this level of error falls within the typical range reported in the technical literature for service life modeling of concrete structures [33].

3.5 Estimation of corrosion initiation of rebar

In Figure 6, the estimated reinforcement corrosion initiation time at a depth of 5 cm is presented. As expected, the time for corrosion initiation in the O-AAS mixture is significantly

longer than that in the OPCC mixture. Additionally, placement in an unsaturated environment has led to a reduction in the estimated time for corrosion initiation. To compare the impact of curing duration before unsaturated exposure on O-AAS versus OPCC corrosion initiation, the estimated times for each mixture were normalized relative to their respective estimated times under W conditions. Figure 7 presents these normalized corrosion initiation times for O-AAS and OPCC under various environmental conditions (relative to condition W).

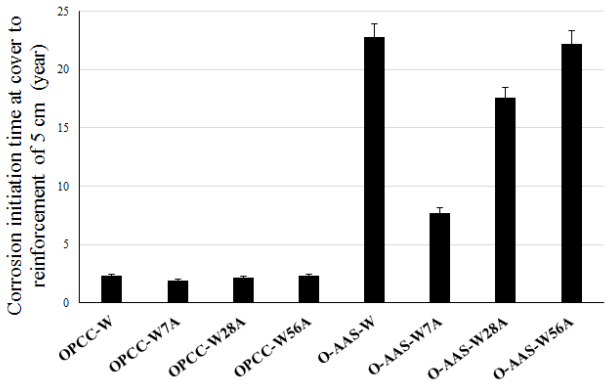

Fig. 6: Predicted corrosion initiation time at 50 mm cover to reinforcement.

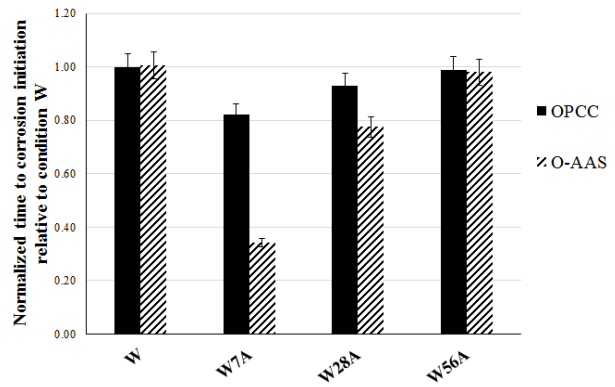

Fig. 7: Normalized predicted corrosion initiation time at 50 mm cover to reinforcement relative to W conditions.

The estimated normalized time to corrosion initiation relative to condition W for the OPCC mixture under conditions W, W7A, W28A, and W56A is 1.0, 0.82, 0.93, and 0.99, respectively. Similarly, the estimated normalized time to corrosion initiation relative to condition W for the AAS mixture under conditions W, W7A, W28A, and W56A is 1.0, 0.34, 0.78, and 0.98, respectively.

These results indicate that unsaturated conditions had a greater impact on the estimated corrosion initiation time of AAS compared to OPCC. Additionally, the estimated corrosion initiation times of OPCC under conditions W, W28A, and W56A are similar to each other, and the estimated corrosion initiation times of O-AAS under conditions W and W56A are also similar to each other. The primary reason for the reduction in the estimated corrosion initiation time in the unsaturated environment with 50% relative humidity is the formation of microcracks due to drying shrinkage.

Therefore, the required curing time to prevent the formation of microcracks caused by drying shrinkage at a relative humidity of 50% has a greater impact on the estimated corrosion initiation time of O-AAS compared to OPCC. The obtained results indicate that to eliminate the influence of the unsaturated environment with a relative humidity of 50% on the estimated corrosion initiation time, the curing periods for OPCC and O-AAS mixtures are 28 and 56 days, respectively.

4. Conclusion

Based on laboratory studies and modeling, the following results were obtained:

-The curing duration of concrete before exposure to an unsaturated environment with 50% relative humidity can influence the properties, especially the permeability, of both OPCC and O-AAS mixtures.

-The 360-day compressive strength of OPCC and O-AAS standard specimens, after 7 days of curing in an unsaturated environment with 50% relative humidity, decreased by 21.0% and 33.2%, respectively, compared to specimens cured under fully saturated conditions.

-The 360-day chloride ion diffusion coefficient of OPCC and O-AAS standard specimens, after 7 days of curing in an unsaturated environment with 50% relative humidity, increased by 22.0% and 155.2%, respectively, compared to standard specimens cured under fully saturated conditions.

-The estimated time to corrosion initiation of OPCC and O-AAS, after 7 days of curing in an unsaturated environment with 50% relative humidity, decreased by 17.8% and 66.0%, respectively, compared to specimens cured under fully saturated conditions.

-The results indicate that a minimum of 28 days of wet curing for OPCC standard specimens, and 56 days for O-AAS standard specimens, eliminates the detrimental effects of exposure to a 50% relative humidity unsaturated environment on their compressive strength and chloride ion diffusion coefficient on standard specimens.

- In general, the results of this study suggest that, for comparable 28-day compressive strength between OPCC and O-AAS mixtures, the required curing duration for O-AAS in practical applications should be at least twice that of OPCC to achieve similar performance regarding changes in strength properties and permeability in unsaturated environments. It should be noted that the findings of this study are specific to O-AAS with sodium metasilicate and exposed to 50% relative humidity. Different activators (e.g., sodium hydroxide, sodium carbonate) or humidity levels

may lead to different curing requirements. Therefore, the recommended 56-day curing period for standard specimens should be considered as a reference for similar mix designs and exposure conditions.

References

[1] Jiang L., Niu Y., Jin W., Gao H., and Chen L., (2022). Influence of chloride salt type on chloride ion diffusion performance of alkali-activated slag mortar, Construct. Build. Mater., 351 128930, https://doi.org/10.1016/J.CONBUILDMAT.2022.128930.

[2] Duzy P., Choinska M., Hager I., Amiri O., Claverie J., (2022). Mechanical Strength and Chloride Ions' Penetration of Alkali-Activated Concretes (AAC) with Blended Precursor. Materials, 15, 4475. https://doi.org/10.3390/ ma15134475

[3] Bagheri A., Ajam A., and Zanganeh H., (2021). Effect of very early age exposure on chloride ingress and service life performance of binary and ternary concretes. Constr. Build. Mater., 289. 123137, https://doi.org/10.1016/j.conbuildmat.2021.123137.

[4] Nasiri S., Madandoust R., Ranjbar M.M., (2023). Investigating the Calcination Temperature and Grinding Time of Calcined Clay on the Mechanical Properties and Durability of LC3 Concrete. Infrastructures, 8, 139. https://doi.org/10.3390/infrastructures8100139

[5] Ehlen, M.A. Life-365 Service Life Prediction Model and Computer Program for Predicting the Service Life and Life-Cycle Cost of Reinforced Concrete Exposed to Chlorides. 2020. User's manual, Version 2.2.3. Produced by the Life-365™ Consortium III. http://www.life-365.org/download/Life-365_v2.2.3_Users_Manual.pdf.

[6] Nasir M., Mahmood A.H., Ashraf A. and Bahraq A.A., (2024). History, recent progress, and future challenges of alkali-activated binders – An overview, Construction and Building Materials, 426, 136141, https://doi.org/10.1016/j.conbuildmat.2024.136141

[7] Elzeadani M., Bompa D.V., and Elghazouli A.Y., (2022). One part alkali activated materials: A state-of-the-art review, Journal of Building Engineering, 57, 104871, https://doi.org/10.1016/j.jobe.2022.104871

[8] Fu Q., Bu M., Zhang Zh., Xu W., Yuan Q., and Niu D., (2023). Hydration Characteristics and Microstructure of Alkali-Activated Slag Concrete: A Review, Engineering, 20, 162–179, https://doi.org/10.1016/j.eng.2021.07.026

[9] Luukkonen T, Alkali-Activated Materials in Environmental Technology Applications, Woodhead Publishing Series in Civil and Structural Engineering, 2022.

[10] Amran M., Onaizi A.M., Makul N., Abdelgader H.S., Tang W.C., Alsulami B.T., Alluqmani A.E., and Gamil Y., (2023). Shrinkage mitigation in alkali-activated composites: A comprehensive insight into the potential applications for sustainable construction, Results in Engineering, 20, 101452, https://doi.org/10.1016/j.rineng.2023.101452

[11] Ye H., and Radlińska A., (2017). Shrinkage mitigation strategies in alkali-activated slag, Cement and Concrete Research, 101, 131–143, http://dx.doi.org/10.1016/j.cemconres.2017.08.025

[12] Wu Z., Wong H.S., and Buenfeld N.R., (2015). Influence of drying-induced microcracking and related size effects on mass transport properties of concrete, Cement and Concrete Research, 68, 35–48, http://dx.doi.org/10.1016/j.cemconres.2014.10.018

[13] Sa C.D., Benboudjema F., Thiery M., and Sicard J., (2008). Analysis of microcracking induced by differential drying shrinkage, Cement & Concrete Composites, 30, 947–956, doi:10.1016/j.cemconcomp.2008.06.015.

[14] Collins FG, and Sanjayan JG., (2000). Microcracking and strength development of alkali activated slag concrete. Cement Concrete Compos., 23(4–5), 345–352. https://doi.org/10.1016/S0958-9465(01)00003-8.

[15] Miao Y., Lu Z., Wang F., Wang H., Li Y., Lin J., and Jiang J., (2023). Shrinkage cracking evolvement in concrete cured under low relative humidity and its relationship with mechanical development, Journal of Building Engineering, 72, 106670, https://doi.org/10.1016/j.jobe.2023.106670

[16] Ogawa Y., Suzuki SH., and Kawai K., (2024). Impact of air exposure post-steam curing on the internal curing efficiency of porous ceramic roof-tile waste fine aggregate in steam-cured fly ash concrete, Materials Letters, 366, 136576, https://doi.org/10.1016/j.matlet.2024.136576

[17] Xia H., Lv X., Wang H., Song L., Zhang G., Cao D., and Chen H., (2024). Shrinkage, mechanical properties and freeze-thaw resistance of cement mortar containing internal curing materials with different absorption behaviors at low humidity, Construction and Building Materials, 416, 135182, https://doi.org/10.1016/j.conbuildmat.2024.135182

[18] Wu Z., Wong H.S., Chen C., and Buenfeld N.R., (2019). Anomalous water absorption in cement-based materials caused by drying shrinkage induced microcracks, Cement and Concrete Research, 115, 90–104, https://doi.org/10.1016/j.cemconres.2018.10.006

[19] El-Hassan H., Shehab E., and Al-Sallamin A., (2018). Influence of Different Curing Regimes on the Performance and Microstructure of Alkali-Activated Slag Concrete. Journal of Materials in Civil Engineering, 30(9), 04018230. doi:10.1061/(asce)mt.1943-5533.0002436

[20] Mohamed, O.A., (2023). Effects of the Curing Regime, Acid Exposure, Alkaline Activator Dosage, and Precursor Content on the Strength Development of Mortar with Alkali-Activated Slag and Fly Ash Binder: A Critical Review. Polymers, 15, 1248. https://doi.org/10.3390/polym15051248

[21] Prinsse S., Hordijk D.A., Ye G., Lagendijk P., and Luković M., (2020). Time-dependent material properties and reinforced beams behavior of two alkali-activated types of concrete, Struct. Concr., 21, 642-658, 10.1002/suco.201900235

[22] Wardhono A, Gunasekara C, Law DW, and Setunge S., (2017). Comparison of long term performance between alkali activated slag and fly ash geopolymer concretes. Construct Build Mater., 143, 272–279. http://dx.doi.org/10.1016/j.conbuildmat.2017.03.153

[23] Dong M., Elchalakani M., and Karrech A., (2020). Development of high strength one-part geopolymer mortar using sodium metasilicate, Construction and Building Materials, 236, 117611, https://doi.org/10.1016/j.conbuildmat.2019.117611

[24] ASTM C150, Standard specification for Portland Cement, ASTM International, Philadelphia, PA, 2017.

[25] ASTM C989, Standard specification for Slag cement for use in concrete and mortars, ASTM International, Philadelphia, PA, 2017.

[26] ASTM C33, Standard specification for concrete aggregates, ASTM International, Philadelphia, PA, 2017.
[27] Marvila M.T., Garcez de Azevedo A.R., Linhares Junior J.A.T., and Vieira C.M.F., (2023). Activated alkali cement based on blast furnace slag: effect of curing type and concentration of Na20, Journal of Materials Research and Technology, 23, 4551–4565, https://doi.org/10.1016/j.jmrt.2023.02.088
[28] ASTM C157, Standard test method for length change of hardened cement mortar and concrete, ASTM International, Philadelphia, PA, 2017.
[29] ASTM C39, standard test method for compressive strength of cylindrical concrete specimens, ASTM International, Philadelphia, PA, 2017.
[30] NT Build 492, Chloride migration coefficient from Non-steady sate migration experiments, NORDTEST, Finland, 1999.
[31] Rahmani K., Nasrollahzadeh K., and Rostami M., (2023). Experimental Study on the Effects of Aggregate Content and Fibers on Mechanical Properties of One-Part Alkali-Activated Slag Concrete, Journal of Concrete Structures and Materials, 8 (2), 146-162.
[32] Bagheri A., Ajam A., and Zanganeh H., (2019). Investigation of chloride ingress into concrete under very early age exposure conditions, Constr. Build. Mater., 225, 801–811, https://doi.org/10.1016/j.conbuildmat.2019.07.225.
[33] Yu X., Li J., Yu Y., and Song A., (2024). Advancing service life estimation of reinforced concrete considering the coupling effects of multiple factors: Hybridized physical testing and machine learning approach, Journal of Building Engineering, 84, 108476, https://doi.org/10.1016/j.jobe.2024.108476